JNTM JOURNAL of NEW TECHNOLOGY and MATERIALS

Journal of New Technology and Materials

Vol. 14, No. 2 (2024), 34–46

RESEARCH ARTICLE

Pore-Preserving Boron Coordination of Palladium on Porous Carbon for Selective Hydrogen Release from Formic Acid

S. Wayne[1,*]

[1]Department of Chemistry, The University of Hong Kong, Hong Kong, China

*Correspondence: 1298323@163.com

Received date: July 28, 2024; Accepted date: November 30, 2024

Abstract

Formic acid acts as a portable hydrogen storage medium, but the ability of formic acid for providing hydrogen on demand relies heavily on dehydrogenation catalysts capable of promoting dehydrogenation reaction efficiently without any undesired carbon monoxide formation via the pathway of formic acid dehydration. In this article, the use of Pd nanoparticles decorated with boron doped pores in carbon support matrix (Pd/BPC) as a structure-tuned catalyst for low temperature formic acid dehydrogenation has been investigated. Specifically, the key research question of this paper addresses whether Pd/BPC shows superior catalytic performance due to pore retention, enhancement in Pd-support interaction, or coupling effect of both. In order to answer such research question, the Pd/BPC catalysts have been evaluated based on final gas evolution amount, specific rate, pore-retention factor, anchoring ratio determined from adsorption energy, surface evidence for mixed valent Pd, and cycleability. Optimal Pd/BPC catalyst shows a BET specific surface area of 530.1 $m^2\,g^{-1}$, pore volume of 3.03 $cm^3\,g^{-1}$, representative pore diameter of 26.3 nm, boron content of 1.3 wt.%, palladium content of 3.0 wt.% and Pd nanoparticle size of approximately 3.6 nm. At 50 °C, this optimal catalyst generates around 105 mL of H_2/CO_2 gas mixture during 90 minutes' period, corresponding to 38.9 $mL\,g^{-1}\,min^{-1}$ gas generation capacity. It corresponds to approximately 2.9 times of Pd/PC and 3.9 times of commercial Pd/C. The BET surface area of the pores and the original carbon remain 79.9%, pore volume remains 86.1%, and representative pore diameter remains 96.3% of the respective original counterparts, leading to a combined pore retention factor of 0.663. Meanwhile, anchoring ratio of Pd increases from 1.00 for pure graphene to 1.04 for nitrogenated graphene to 2.34 for B-graphene. The enhanced activity cannot be simply attributed to the increase in surface area.

Keywords: formic acid, hydrogen release, palladium catalyst, boron-doped porous carbon, metal–support interaction, mesoporosity, dehydrogenation selectivity, nanostructured carbon

1 Introduction

A technology capable of using hydrogen in low-carbon energy conversion relies not only on efficient hydrogen production but also on proper hydrogen storage, transportation and release. Compressed and liquid hydrogen storage technologies are well developed, however, they are constrained by requirements for pressure vessel and liquefaction as well as boil-off problems that complicate their application in portable and decentralized devices. On the other hand, hydrogen released from chemicals offers an interesting alternative for such applications because hydrogen can be stored chemically in molecular bonds and catalytically released nearby. Formic acid stands out as an exemplary chemical carrier because it is a liquid substance at room temperature, soluble in water, easy to handle and recyclable as a part of a carbon-neutral carbon cycle. Namely, carbon dioxide can be hydrogenated or reduced to formate and formic acid via electrochemical reduction [1–3]. While its hydrogen content per unit mass is not higher than for compressed hydrogen, the possibility of liquid handling and direct catalytic conversion makes it relevant for a hydrogen storage application.

However, the chemistry involved in formic-acid dehydrogenation requires careful design of the catalyst. Formic acid molecules can follow two main pathways: dehydrogenation producing hydrogen and carbon dioxide and dehydration

yielding carbon monoxide and water. Carbon monoxide has an undesirable effect on heterogeneous catalysts: it strongly interacts with noble metal surfaces making the reaction inactive and poisoning polymer-electrolyte fuel cell anodes in the case of electrocatalysts. Hence, a good catalyst not only produces gas from formic acid but also selects the dehydrogenation pathway and does not produce any carbon monoxide. Palladium-based catalysts show promise in this regard because they catalyze reactions of this type easily under mild aqueous conditions and have potential for very high selectivities if particle size, electronic state and support are tuned correctly [4–6]. However, if palladium is unsupported or poorly supported, its particles tend to aggregate and block catalytic sites, making the support crucial for the catalyst.

The properties required from the support include large specific surface area, chemical and thermal stability, good electrical conductivity and a controllable porous texture. Porous carbon supports are the choice here due to their high surface area, chemical stability and electrical conductivity. However, while high specific surface area is often desirable, a high portion of surface in micropores may lead to decreased catalytic activity because only a limited number of formic acid or formate molecules will reach those pores. On the other hand, pores blocked by deposited metal will make catalytic sites inaccessible even if the porosity is high. Thus, the most important property of the support is the retention of pore volume and characteristic pore diameters, i.e., pore texture. Since the process of formic-acid decomposition is multiphase in nature with a liquid reagent, solid catalyst and gas products, the catalytic system must be optimized by taking the porosity into account.

In addition, heteroatom doping of carbon creates an active interfacial region on top of the purely textural carbon support. Doping with heteroatoms alters the electronic state of the carbon lattice and can modify the distribution of noble metal nanoparticles. Nitrogen-doped carbons have been extensively studied in recent years due to pyridinic, pyrrolic and graphitic nitrogen groups' ability to affect electronic structure and stabilize nanoparticles [7–9]. Boron doping creates an opposite effect: being less electronegative than carbon, boron introduces holes into carbon structures creating an additional interaction force between carbon and palladium atoms. This effect could prove valuable in preventing palladium nanoparticles' aggregation and diffusion leading to a decrease in effective surface area. There have been some previous studies investigating B-Pd systems in context of catalyzing formic acid dehydrogenation, revealing changes in Pd's electronic state, higher catalytic activity and changes in intermediate affinity in a similar electrocatalyst application [10–12]. Thus, the question is no longer whether boron is helpful or not but how its incorporation modifies the performance of Pd catalyst.

Most recently, a number of papers addressing performance improvements in Pd catalysts in aqueous formic acid dehydrogenation have appeared, exploring different ways of improving activity and selectivity. These include bimetallization of palladium nanoparticles, functionalization of the carbon substrate and creation of hierarchical porous substrates [13–15]. One of the key insights from these studies is that high catalytic performance is achieved by optimizing the whole system including metal particles, support and reaction environment. At the same time, most comparison analyses are still based on quantitative measures like turnover frequencies or yield of released gas but lack similar quantitative data regarding the preservation of pore volume, anchoring efficiency and selectivity. Hence, it becomes impossible to distinguish three potential sources of improved catalytic performance: more accessible pore channels, better anchoring of particles and increased selectivity.

In this paper, we try to answer this question in the case of Pd-BPC catalysts where carbon support was modified with boron atoms. A numerical database provided in this paper corresponds to the published study about a family of Pd/BPC catalysts synthesized from porous carbon derived from petroleum asphalt, doped with boron, loaded with palladium and subjected to formic-acid dehydrogenation [20]. A major result obtained in this study is that the optimal Pd/BPC catalyst created from a carbon-boron molar ratio 1:5, calcination at 900 °C and reduction at 60 °C has the highest catalytic performance. We advance this analysis by considering a particular material question: *Can the high hydrogen release performance of the optimal Pd/BPC catalyst be attributed solely to pore conservation, anchoring or both effects simultaneously?*

2 Materials and Methods

2.1 Catalyst system and the basis of analysis

The catalysts to be compared are boron-doped porous carbon containing palladium (Pd/BPC), nitrogen-doped porous carbon containing palladium (Pd/NPC), undoped porous carbon containing palladium (Pd/PC), commercial Pd/C and its counterparts without the metal component. The carbon catalyst was made by templating petroleum asphalt, followed by doping with B or N and further deposition of Pd on the resultant carbon matrix. Formic acid solution (50 °C, 30 mg, 90 min) was employed as the catalytic testing medium. The parameters analysed herein include BET specific surface area, pore volume, typical pore diameter, content of B and Pd, Pd nanoparticle size, gas volume released, Pd surface state, cycling performance and adsorption energy of Pd on model carbon surfaces.

The need for rearranging these data is dictated by our intention to articulate an argument of structure versus activity. The activity order alone singles out Pd/BPC as the best performing catalyst, yet it fails to answer the question as to what causes the difference in catalytic activities. In view of this, the present analysis involves three different levels: texture

that dictates liquid access; interfacial anchoring that controls Pd stability; and catalytic efficiency, which verifies that the structural advantages are indeed reflected by hydrogen generation ability.

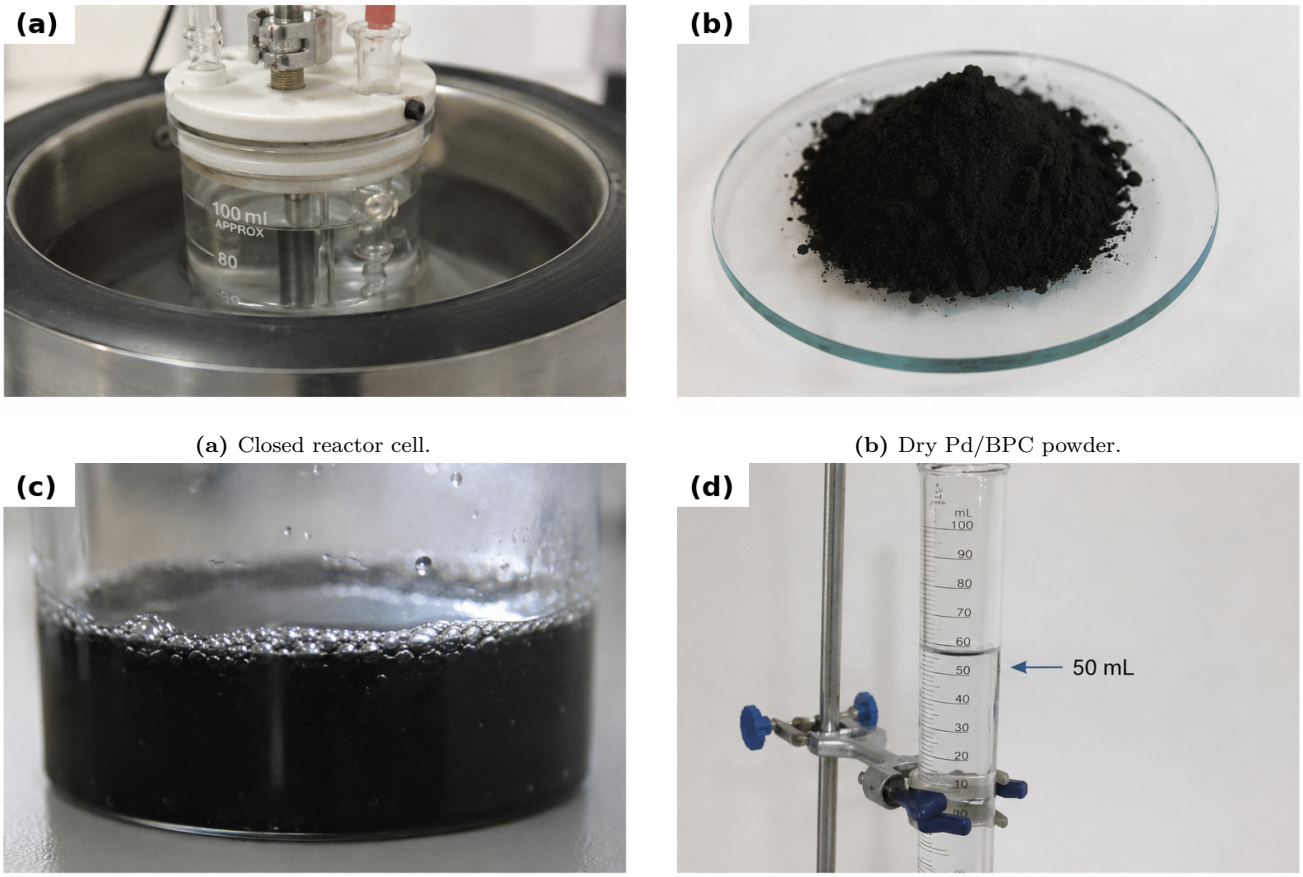

(a) Closed reactor cell.

(b) Dry Pd/BPC powder.

(c) Aqueous catalytic slurry.

(d) Gas-collection readout.

Figure 1. Reaction and catalyst context for the formic-acid dehydrogenation comparison. The panels record the sealed glass reactor, the recovered black Pd/BPC powder, the catalyst suspension during aqueous reaction and the volumetric collection of generated gas.

Figure 1 is critical since the measured response is not an idealized vacuum-surface reaction but a real-world gas-evolution response. The slurry picture proves that the catalyst works in a liquid medium. Hence, pore accessibility and particle wetting must be accounted for. Finally, the gas collection panel reveals why the analysis relies on volumetric productivity – the experiment is a measure of gas production over a fixed period of time. This figure, therefore, provides a foundation for describing catalyst performance within the measurement protocol.

2.2 Definitions of productivity descriptors and physical interpretation

The apparent volumetric gas generation rate, R_V, was computed from the endpoint gas volume as

$$R_V = \frac{V_{90}}{t}, \tag{1}$$

where V_{90} is the total volume of produced H_2/CO_2 gas at the endpoint, namely, at 90 min reaction time, and t is the actual reaction time. Eq. (1) is deliberately straightforward but is not an intrinsic kinetic constant. This descriptor is independent of Pd dispersion, Pd surface exposure, concentration of dissolved formate, solubility of gases and any mass transfer resistances. It is, rather, a productivity descriptor that makes comparison of the catalyst series possible under the same experimental conditions in terms of reactor volume, mass of the catalyst charged, and time span. The volumetric productivity for Pd/BPC amounts to $R_V = 105/90 = 1.17\,\mathrm{mL\,min^{-1}}$. It is considerably higher than that of commercial Pd/C.

The catalyst mass-normalized productivity R_m was estimated from

$$R_m = \frac{V_{90}}{m_{cat}t}, \tag{2}$$

where $m_{cat} = 0.030\,\mathrm{g}$. With this equation, the effect of catalyst mass on gas productivity is removed, and gas generation efficiency is assessed in terms of gas volume per unit mass per unit time. This is very useful in this case where all catalysts are tested using equal catalyst masses. Specifically, $R_m = 105/(0.030 \times 90) = 38.9\,\mathrm{mL\,g^{-1}\,min^{-1}}$ for Pd/BPC. This descriptor makes clear that high catalytic activity is due to increased catalyst efficiency, not due to higher mass charge.

2.3 Descriptor for pore conservation

In order to verify whether boron modification and Pd doping maintain internal transport features of the initial porous structure of porous carbon, we introduce a pore conservation factor

$$\Pi_p = \left(\frac{S_{BET}^{Pd/BPC}}{S_{BET}^{PC}}\right)\left(\frac{V_p^{Pd/BPC}}{V_p^{PC}}\right)\left(\frac{D_p^{Pd/BPC}}{D_p^{PC}}\right), \tag{3}$$

where S_{BET}, V_p and D_p stand for BET specific surface area, pore volume, and average pore diameter, respectively. Multiplication in the above formula makes it strictly demanding. Catalyst whose one textural parameter is conserved but other(s) lost gets a low value of Π_p. This is justified for the liquid phase reactions, as access to the surface is dependent on maintaining the whole pore structure. Thus, for Pd/BPC in comparison with parent porous carbon, $\Pi_p = (530.1/663.5)(3.03/3.52)(26.3/27.3) = 0.663$. It does not imply that two thirds of each particular pore are preserved but summarizes the overall maintenance of the accessible pore structure after boron modification and metal loading.

2.4 Descriptor for metal-support interaction

The effect of porous carbon as the support on Pd stabilization was characterized via a descriptor of Pd–support anchoring strength, Θ_{MSI}. This descriptor was estimated based on calculated Pd adsorption energies,

$$\Theta_{MSI} = \frac{|E_{ad}^{modified}|}{|E_{ad}^{graphene}|}. \tag{4}$$

It is a ratio between the absolute values of calculated Pd adsorption energy onto doped carbon model and pure graphene. A value exceeding unity signifies stronger metal support interaction than pristine graphite. Importantly, Θ_{MSI} cannot be directly interpreted as a rate law in catalytic reactions. Indeed, stronger metal anchoring facilitates Pd stabilization but may impair catalytic properties of the system. Thus, the proposed descriptor should always be complemented by the results of catalytic testing. For this type of catalysts, Θ_{MSI} must be combined with gas evolution efficiency, pore conservation factor and selectivity.

2.5 Reaction pathway and selectivity criterion

The intended reaction is the dehydrogenation of formic acid:

$$\mathrm{HCOOH} \longrightarrow \mathrm{H_2} + \mathrm{CO_2}. \tag{5}$$

Eq. (5) is relevant as it describes the desired product couple and, thus, hydrogen release from the reaction solution. Also, it explains why the gas volume measured must only be meaningful in terms of selectivity. If the formate dehydrogenation proceeds selectively, gas evolution means hydrogen generation with concurrent CO2 formation. Depending on applications, both products are either acceptable or the CO2 is further converted to hydrogen, i.e., methane.

Eq. (6) shows the undesirable competing reaction path.

$$\mathrm{HCOOH} \longrightarrow \mathrm{CO} + \mathrm{H_2O}. \tag{6}$$

Eq. (6) is included because it sets the principal constraint on catalyst design. A catalyst that maximizes gas evolution by allowing CO formation would be unsuitable for fuel-cell-linked hydrogen supply and could deactivate itself through CO adsorption on Pd. The absence of detected CO for the boron-modified catalyst is therefore treated as a necessary performance condition rather than a secondary observation. The ranking of catalysts in this paper consequently considers productivity, pore retention, anchoring strength and selectivity together.

3 Results and Discussion

3.1 Textural integrity of the boron-modified porous carbon support

The first part of the research question concerns transport: does Pd/BPC remain sufficiently porous after boron incorporation and palladium loading? Table 1 gives the structural and compositional values used to answer this point. The parent porous carbon has a BET surface area of 663.5 $m^2\,g^{-1}$, pore volume of 3.52 $cm^3\,g^{-1}$ and representative pore diameter of 27.3 nm. After boron modification and Pd deposition, Pd/BPC retains 530.1 $m^2\,g^{-1}$, 3.03 $cm^3\,g^{-1}$ and 26.3 nm, respectively. The decrease is measurable but not destructive, indicating that the support does not lose the mesoporous character required for liquid-phase operation.

Table 1. Textural, compositional and particle-size values used to evaluate pore conservation in the Pd/BPC catalyst.

Material	S_{BET} ($m^2\,g^{-1}$)	Pore diameter (nm)	Pore volume ($cm^3\,g^{-1}$)	B content (wt.%)	Pd content (wt.%)	Pd particle size (nm)
PC	663.5	27.3	3.52	–	–	–
Pd/BPC	530.1	26.3	3.03	1.3	3.0	3.6

Table 1 shows that Pd deposition occurs without catastrophic filling or collapse of the pore system. The most striking value is the preservation of the representative pore diameter: 26.3 nm remains after catalyst preparation, corresponding to 96.3% of the parent value. This matters because pore diameter controls whether solvated formic acid, formate and product gas can move through the internal support. The table also links texture with metal dispersion: the retained mesoporosity coexists with a representative Pd particle size of about 3.6 nm, suggesting that open transport and nanoscale metal placement are achieved simultaneously rather than traded against one another.

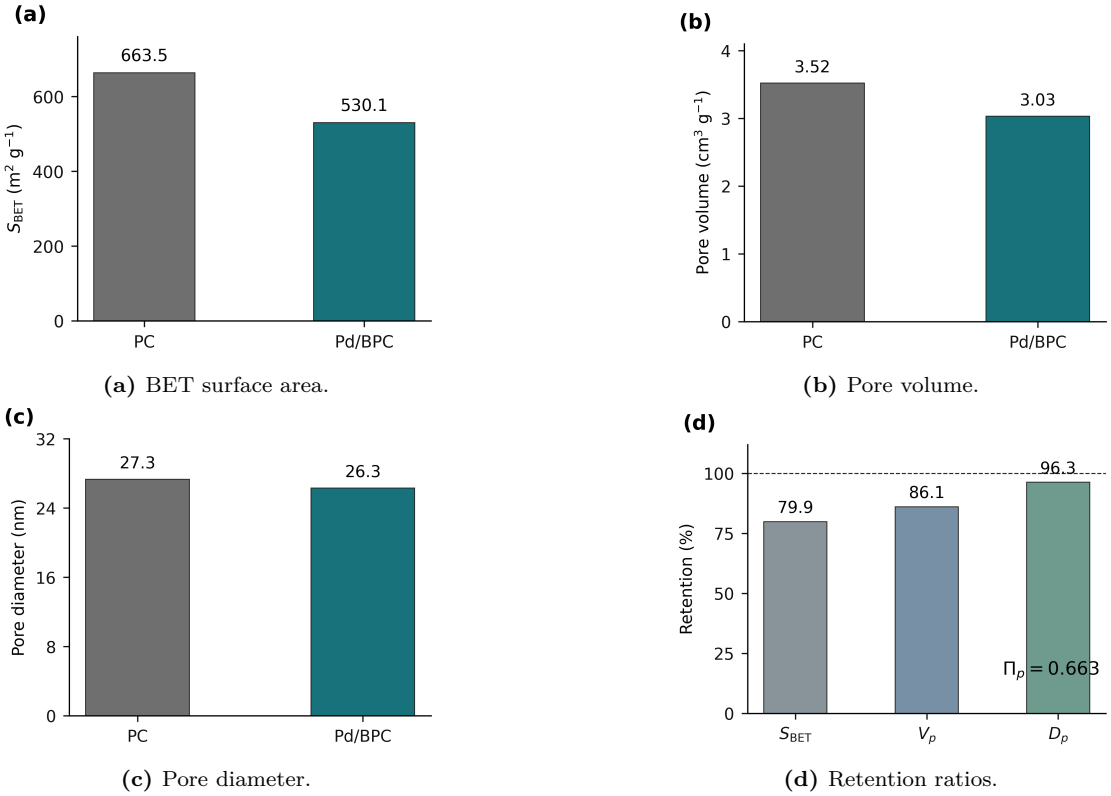

(a) BET surface area. **(b)** Pore volume. **(c)** Pore diameter. **(d)** Retention ratios.

Figure 2. Textural comparison between parent porous carbon and Pd/BPC. The four panels compare retained BET surface area, pore volume, representative pore diameter and the combined pore-conservation factor after boron modification and Pd incorporation.

Figure 2 converts the tabulated values into a direct visual argument. The BET surface area decreases more than the pore diameter, which is expected when metal particles and heteroatom functionalities occupy part of the internal surface. However, the pore-volume and diameter retention values remain high enough to support the interpretation that reactant transport is maintained. The combined factor of 0.663 is therefore not a trivial number; it shows that Pd/BPC preserves a large fraction of the pore architecture while introducing catalytically relevant Pd and boron sites. The figure answers the transport part of the research question by showing that Pd/BPC is not merely active because it contains Pd, but because Pd is placed on a support that remains liquid-accessible.

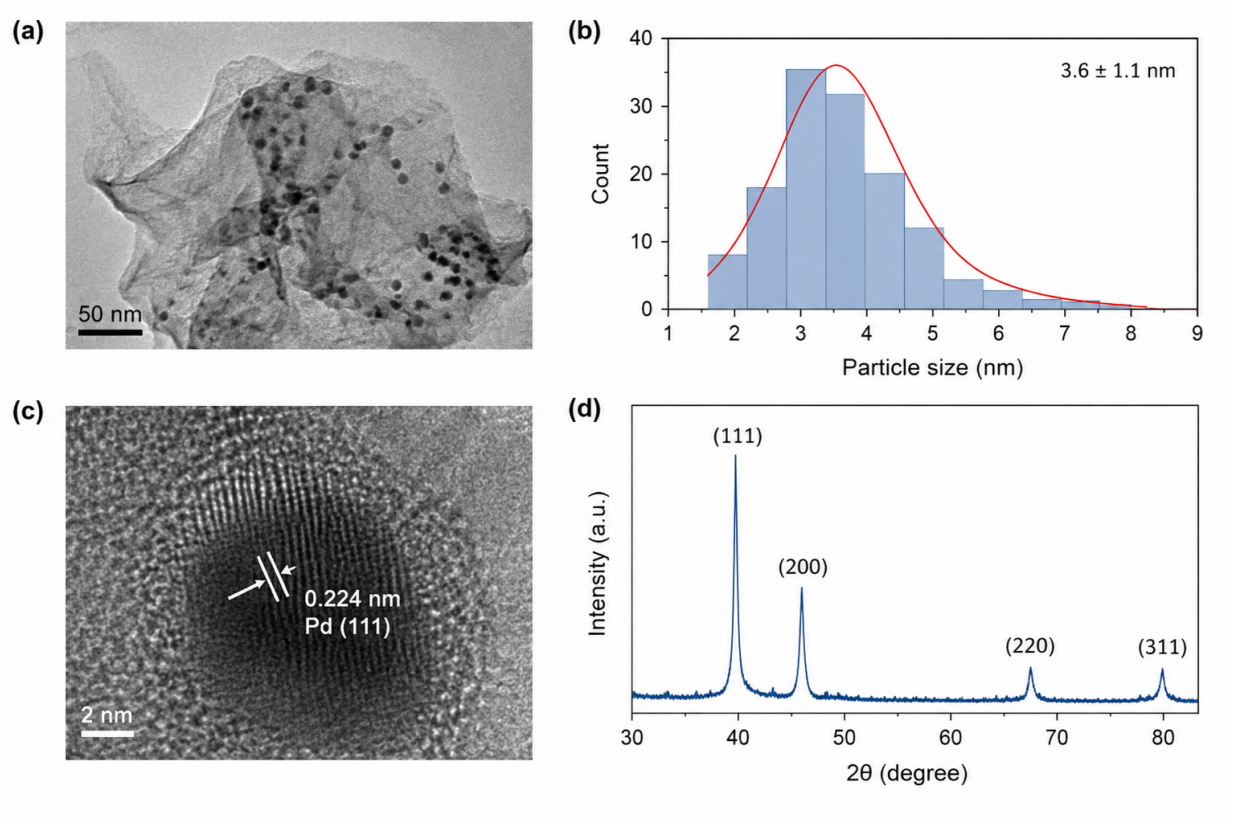

Figure 3. Microstructural and phase evidence for the Pd/BPC catalyst. The TEM image, particle-size distribution, high-resolution lattice image and diffraction pattern support the presence of nanoscale Pd domains distributed on the porous carbon support.

Figure 3 provides the microstructural counterpart to the adsorption data. The particle-size distribution centred near the value used in Table 1 indicates that Pd is present as nanoscale domains rather than as large, poorly dispersed aggregates. This observation is essential because pore conservation alone would not guarantee high catalytic activity if the Pd phase were sparse, blocked or agglomerated. The diffraction and lattice information further support the assignment of palladium-containing crystalline domains on the carbon substrate. Taken together with Figure 2, the microstructural evidence supports the first part of the mechanism: Pd/BPC preserves accessible mesoporosity while hosting small Pd particles.

3.2 Endpoint gas productivity and catalyst ranking

The second part of the research question asks whether the preserved pore structure and Pd placement translate into measurable hydrogen-release productivity. Table 2 summarizes the endpoint gas volumes and normalized productivity values for the catalyst series. Pd/BPC produces approximately 105 mL of gas in 90 min, while Pd/NPC, Pd/PC and commercial Pd/C produce 58 mL, 36 mL and 27 mL, respectively. Normalization by the 0.030 g catalyst charge gives $38.9\,\mathrm{mL\,g^{-1}\,min^{-1}}$ for Pd/BPC.

Table 2. Endpoint gas-evolution values and normalized productivity for the formic-acid dehydrogenation comparison.

Catalyst	V_{90} (mL)	R_V (mL min^{-1})	R_m (mL g^{-1} min^{-1})	Relative to Pd/C
Pd/BPC	105	1.17	38.9	3.89
Pd/NPC	58	0.64	21.5	2.15
Pd/PC	36	0.40	13.3	1.33
Commercial Pd/C	27	0.30	10.0	1.00

Table 2 shows that the boron-modified catalyst is not only marginally better than the controls. Its normalized productivity is nearly four times that of commercial Pd/C and almost three times that of Pd/PC. The comparison with Pd/PC is especially informative because both catalysts use porous carbon as the support logic. Replacing undoped porous carbon with boron-modified porous carbon therefore changes the catalytic response far more strongly than would be expected from a small variation in carbon texture alone. The Pd/NPC result is also informative: nitrogen improves activity relative to Pd/PC, but it does not reach the Pd/BPC level. The ranking therefore points to a boron-specific interfacial effect.

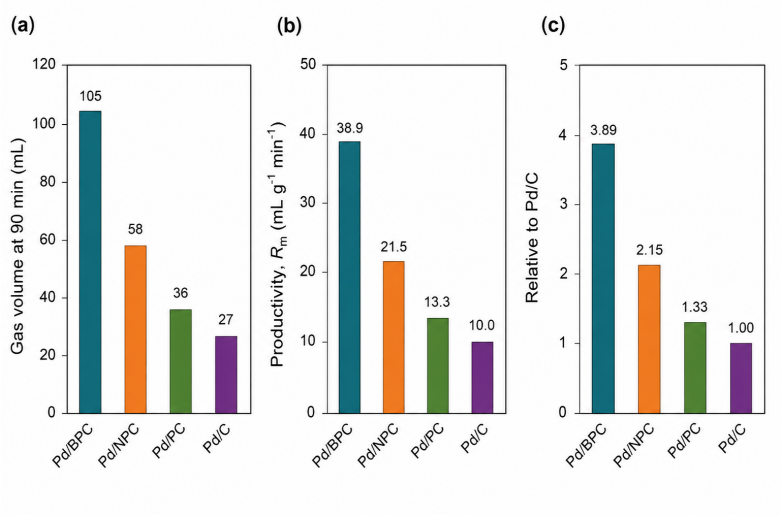

Figure 4. Endpoint catalytic comparison after 90 min. Pd/BPC gives the highest accumulated gas volume, the largest catalyst-mass-normalized productivity and the highest performance ratio relative to commercial Pd/C.

Figure 4 makes the activity hierarchy visually explicit. The bar ranking rules out two incomplete explanations. First, the result cannot be attributed only to the presence of Pd, because all Pd-containing catalysts do not perform equally. Second, it cannot be attributed only to using porous carbon, because Pd/PC remains much less active than Pd/BPC. The figure supports a coupled explanation in which boron modification changes how Pd interacts with the support while the mesoporous carbon network keeps the active domains accessible.

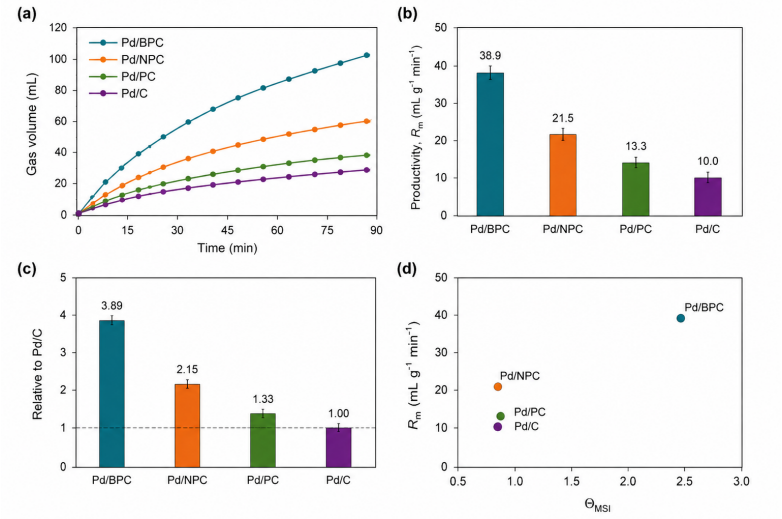

Figure 5. Time-resolved catalytic and descriptor-based comparison of the Pd/porous-carbon catalysts. The gas-evolution curves, productivity bars, relative activity values and pore-conservation relationship show that the boron-modified support combines fast gas release with retained textural accessibility.

Figure 5 adds a dynamic and descriptor-based perspective to the endpoint values. The time-resolved profile is important because a catalyst can show a favourable endpoint through a short initial burst followed by rapid decay, or through sustained gas generation over the full interval. The descriptor panel indicates that Pd/BPC maintains the strongest cumulative response across the measurement period while also occupying the favourable region of the pore-conservation/productivity comparison. This supports the interpretation that the high endpoint volume is not an artefact of a single measurement point. It reflects a catalyst architecture that remains active under the liquid-phase reaction conditions.

3.3 Reduction temperature, Pd valence and surface activation

The preparation route determines whether Pd is reduced sufficiently, dispersed adequately and electronically coupled to the support. Figure 6 compares the reduction-temperature conditions and recovered catalyst appearance. The observed performance trend is consistent with an optimum near 60 °C: lower temperature may leave Pd precursor species less completely converted, whereas excessive temperature may promote uncontrolled growth or less uniform deposition. The reduction step is therefore not a minor synthetic detail; it establishes the Pd surface population that participates in formate activation.

(a) Reduction at 0 °C.

(b) Reduction at 60 °C.

(c) Reduction at 80 °C.

(d) Recovered Pd/BPC powder.

Figure 6. Photographic comparison of reduction-temperature conditions and recovered Pd/BPC powder. The panels document the processing window used to balance Pd reduction, particle distribution and preservation of catalyst morphology.

Figure 6 should be interpreted as process evidence rather than as decorative imagery. The temperature series shows that catalyst performance depends on the chemical history of Pd deposition. The 60 °C condition is significant because it provides enough thermal energy for methanol-assisted reduction while avoiding the harsher conditions that may reduce dispersion. The recovered black powder also confirms that the catalyst retains the macroscopic form needed for slurry operation and repeated handling.

The surface electronic state further clarifies why the reduction condition matters. The Pd 3d features near 335.7 eV and 341.0 eV are assigned to Pd(0), while features near 337.2 eV and 342.5 eV are assigned to Pd(II). A mixed Pd(0)/Pd(II) surface can be beneficial because metallic Pd ensembles facilitate hydrogen recombination, while more electron-deficient Pd centres and neighbouring B/C sites can stabilize formate-like intermediates. The optimum catalyst therefore appears to operate through a surface in which metallic and partially oxidized Pd environments are both present.

Figure 7 strengthens the mechanism by linking performance to surface chemistry. The Pd 3d assignment indicates that Pd/BPC is not a purely metallic Pd powder deposited on carbon. It is an interfacial catalyst with mixed Pd states influenced by the boron-containing carbon matrix. The infrared features support the presence of carbon-framework and functional-group environments that can participate in adsorption and local charge redistribution. The figure therefore answers the electronic part of the research question: boron modification contributes by changing the Pd-support interface, not merely by increasing external surface area.

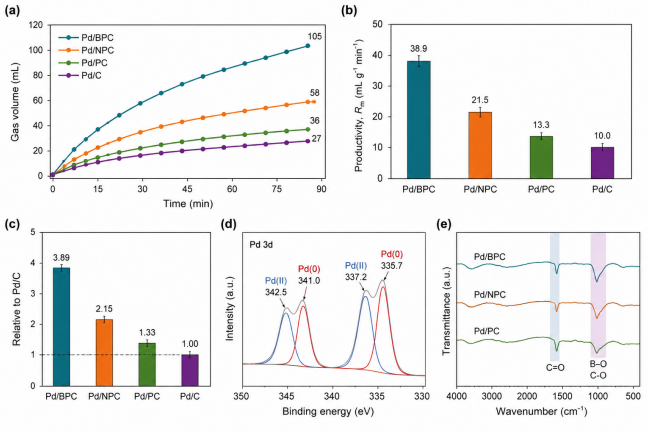

Figure 7. Integrated catalytic and surface-chemistry evidence for Pd/BPC. The gas-evolution profile, normalized productivity, relative activity, Pd 3d mixed-valence assignment and infrared bands connect catalytic output with the Pd/B/C interfacial environment.

3.4 Boron-specific Pd anchoring

Table 3 gives the calculated Pd adsorption energies on undoped graphene, N-graphene and B-graphene model surfaces. The Pd adsorption energy on B-graphene is −1.10 eV, compared with −0.49 eV on N-graphene and −0.47 eV on undoped graphene. The corresponding anchoring ratio is 2.34 for B-graphene, 1.04 for N-graphene and 1.00 for graphene.

Table 3. Adsorption-energy-derived Pd anchoring values on model carbon surfaces.

Support model	Representative catalyst	E_{ad} (eV)	Θ_{MSI}
Graphene	Pd/PC	-0.47	1.00
N-graphene	Pd/NPC	-0.49	1.04
B-graphene	Pd/BPC	-1.10	2.34

According to Table 3, boron and nitrogen are not equal modifiers regarding the strength of Pd adsorption compared to the pristine carbon material. While nitrogen leads to a modest improvement compared to the undoped control, boron increases the adsorption energy significantly, surpassing the two-fold change. This difference between nitrogen and boron explains the performance difference between Pd/NPC and Pd/BPC. The latter benefits from the introduction of boron, which creates electron-deficient regions for stronger Pd binding and better charge redistribution at the Pd–support interface.

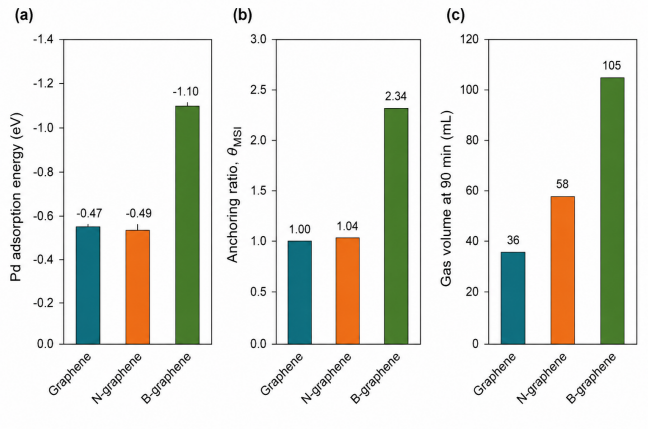

Figure 8. Comparison of adsorption energies, anchoring ratios and gas evolution performance in Pd/PC, Pd/NPC and Pd/BPC. The graph indicates a correlation between anchoring ratio and gas yield and shows the dominance of Pd/BPC due to a stronger metal-support interaction.

As seen in Figure 8, the anchoring ratio is correlated with gas-production rate within the three tested samples. In other words, an increase in the ratio coincides with higher gas-evolution performance. Such data supports the idea of a stronger Pd-metal–support interface providing an increased number of active sites available for reactions and better stabilization of these sites over time. One should exercise caution in this regard, however. While adsorption energy can be a useful

indicator of catalytic performance, it does not necessarily prove any rate law. Additionally, overly strong interaction may negatively impact the ability of a catalytic material to produce products. In this particular case, the strongest anchoring coincides with the greatest productivity and preserved selectivity. Therefore, one can conclude that Pd/BPC operates in the favorable regime, where the active Pd nanoparticles are effectively stabilized by the boron-modified support.

3.5 Coupled pore–anchoring mechanism

It can be seen that the above evidence does not support the single-descriptor mechanism and instead supports a combination of descriptors. Specifically, the porosity-conservation ratio demonstrates that the structure of a carbon material is largely preserved after boron doping and subsequent Pd addition. TEM images demonstrate the presence of Pd nanoparticles with the size close to the nanoparticulate regime. Finally, anchoring ratio data show that boron doping provides substantially higher interaction between the catalytically active Pd and a support. Gas-production rate values confirm the importance of such structural characteristics for enhanced productivity. All of those descriptors are integrated in Figure 9.

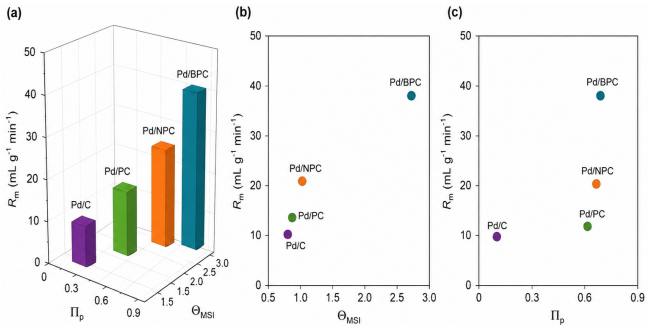

Figure 9. Combined graph indicating a relationship between pore conservation, Pd anchoring and catalytic productivity. According to the graph, Pd/BPC is characterized by a high productivity value and pore conservation.

As seen in Figure 9, a catalyst with high productivity but low pore conservation would demonstrate a dominant role of external Pd nanoparticles and a short-lived surface effect. Similarly, a catalyst with high pore conservation but low productivity would not utilize the existing mesoporous network efficiently. On the contrary, Pd/BPC occupies a favourable point in the descriptor space. As the plot implies, the productivity of this material depends on the combination of retained porosity and efficient Pd anchoring.

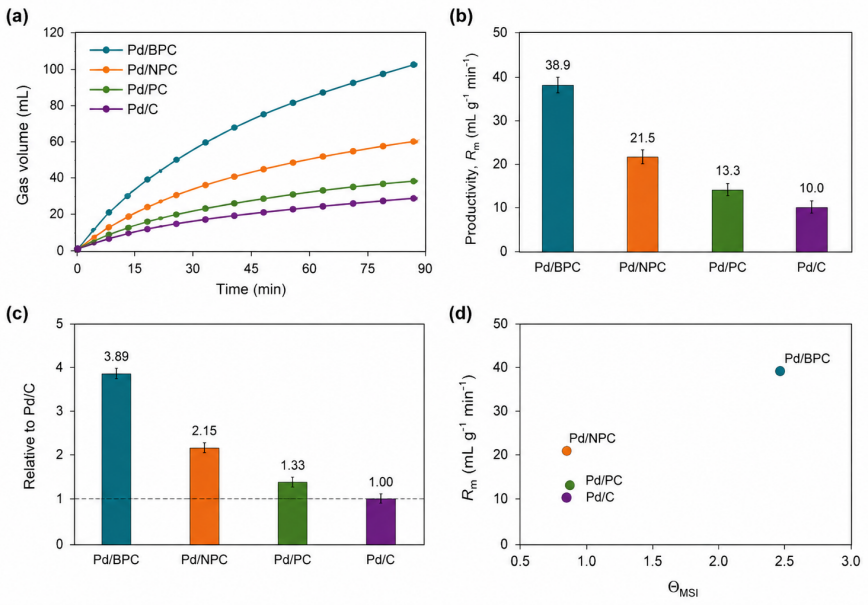

Figure 10. Cyclic gas evolution data, pore conservation, productivity and relative activity in Pd/BPC catalyst. The data demonstrate a relationship between retained porosity and anchoring of Pd in a support.

A mechanism responsible for the performance of Pd/BPC can be described in sequential terms. First, the mesoporous carbon retains its ability to admit aqueous formic acid/formate molecules while allowing the gaseous reaction products to escape with limited pore clogging. Second, boron modification increases the electron deficiency at the support and leads to higher Pd interaction with carbon. Third, a combination of boron-rich and metallic carbon domains provides suitable locations for formate adsorption and C–H activation. Fourth, mixed Pd(0)/Pd(II) surface composition provides additional tuning of Pd catalytic activity through a creation of complementary active sites.

Figure 10 provides information that can help evaluate the stability of Pd nanoparticles inside the Pd/BPC material. Namely, if a material demonstrated high productivity but did not exhibit cyclic behavior, it would likely imply unstable nanoparticles that migrated or were deactivated upon contact with an aqueous medium. On the other hand, the ability of Pd/BPC to demonstrate stable performance suggests the presence of Pd–B/C bonds preventing such processes. At the same time, the ability to retain porosity is a separate descriptor. It is required for the preservation of transport performance and productivity, as the catalyst cannot exhibit high productivity if the liquid access is blocked.

3.6 Implications, limitations and design rules

There are several key conclusions that can be drawn from the study and used as guidelines in future research. First, evaluation of heteroatom-modified porous carbon should take place after Pd addition and not before. Otherwise, the surface area may be overestimated if pores are closed or clogged. Second, one should choose the proper type of heteroatom. In this example, nitrogen modification was more effective than leaving carbon unperturbed. Boron, in turn, led to a larger anchoring ratio. Third, the reduction step is critical for catalytic materials. Pd valency state, Pd nanoparticle size and anchoring depend heavily on the reduction process. Fourth, all of those descriptors should be used in catalyst characterization. In the current case, productivity is not sufficient for determining the exact cause of the improvement.

There are also some significant limitations related to the methodology. The productivity values presented in the study represent the engineering endpoint and should not be overinterpreted as intrinsic turnover frequencies. DFT calculations involve simplified support surfaces and neglect heteroatoms' configuration and other defects. Pore-conservation ratio provides a quick way to analyze the structural performance of the catalyst, but it is no replacement for a detailed pore-size distribution analysis. Consequently, further studies should employ infrared or X-ray absorption spectroscopy. Additional analysis will be needed to reveal the actual state of the catalyst's surface.

One can now provide an explicit answer to the research question. The improved performance of Pd/BPC does not come from the pore conservation only because Pd/PC also demonstrates high retention of mesoporous structure, but does not demonstrate a similar increase in productivity. At the same time, it does not come from the anchoring ratio either. In the current setting, Pd–carbon interaction should occur inside the liquid-accessible pores. Thus, the only logical conclusion is that the advantage stems from the combined effect of these two factors. Retention of mesoporous network guarantees that liquid can be transported to and from the support. Meanwhile, boron induces strong interaction between Pd nanoparticles and a surface and creates suitable active sites. It leads to a relatively fast H_2 production in Pd/BPC.

4 Conclusion

This paper presents a pore-conservation and Pd-anchoring interpretation for Pd catalysts supported on heteroatom-modified porous carbon in a process of low-temperature formic-acid dehydrogenation. The research question was formulated around the problem of identifying the factors responsible for a higher productivity of Pd/BPC catalyst. According to the obtained evidence, this material demonstrates high productivity because it possesses two key characteristics: retained mesoporous channels and a special Pd–boron-carbon surface. Specifically, Pd/BPC retained 79.9% of surface area, 86.1% of pore volume and 96.3% of average pore diameter of Pd/BPC sample. Its pore-conservation ratio equals 0.663, demonstrating that boron doping and Pd adsorption do not eliminate mesoporosity.

Experimental results showed that Pd/BPC releases gas volume of 105 mL during 90 minutes of exposure to formic acid. As a result, the productivity of this catalyst amounts to 38.9 $\mathrm{mL\,g^{-1}\,min^{-1}}$, which is 2.9 and 3.9 times higher than Pd/PC and commercial Pd/C catalysts. When comparing to Pd/BPC and Pd/PC, one can observe that there is an essential difference in the level of improvement caused by each modification type. As Table 3 illustrates, Pd adsorption on a B/graphene surface is −1.10 eV with anchoring ratio of 2.34. Undoped and nitrogen-modified carbons demonstrate anchoring ratios of 1.00 and 1.04 correspondingly.

Consequently, the productivity advantage of Pd/BPC lies in the ability to retain mesopores during processing and create special interfaces with boron atoms leading to increased stability and reactivity of Pd nanoparticles. Mesopores allow transporting aqueous formic acid molecules to and gaseous reaction products from the active sites, while Pd–boron interactions prevent deactivation and migration of the metal. Mixed valency state of Pd nanoparticles is consistent with hydrogen-recombination sites and intermediate-formate-active environments. The lack of detectable CO confirms that the catalyst is capable of producing clean H_2.

Data Availability

All numerical values used for productivity, pore-conservation and anchoring calculations are included in the tables and equations of this article.

Conflicts of Interest

The author declares no conflict of interest.

References

[1] Enthaler, S.; von Langermann, J.; Schmidt, T. Carbon dioxide and formic acid–the couple for environmental-friendly hydrogen storage? *Energy Environ. Sci.* 2010, *3*, 1207–1217.

[2] Fellay, C.; Dyson, P.J.; Laurenczy, G. A viable hydrogen-storage system based on selective formic acid decomposition with a ruthenium catalyst. *Angew. Chem. Int. Ed.* 2008, *47*, 3966–3968.

[3] Yadav, M.; Xu, Q. Liquid-phase chemical hydrogen storage materials. *Energy Environ. Sci.* 2012, *5*, 9698–9725.

[4] Tedsree, K.; Li, T.; Jones, S.; Chan, C.W.A.; Yu, K.M.K.; Bagot, P.A.J.; Marquis, E.A.; Smith, G.D.W.; Tsang, S.C.E. Hydrogen production from formic acid decomposition at room temperature using a Ag–Pd core–shell nanocatalyst. *Nat. Nanotechnol.* 2011, *6*, 302–307.

[5] Mori, K.; Dojo, M.; Yamashita, H. Pd and Pd–Ag nanoparticles within a macroreticular basic resin: An efficient catalyst for hydrogen production from formic acid decomposition. *ACS Catal.* 2013, *3*, 1114–1119.

[6] Kim, Y.; Kim, S.H.; Ham, H.C.; Kim, D.H. Mechanistic insights on aqueous formic acid dehydrogenation over Pd/C catalyst for efficient hydrogen production. *J. Catal.* 2020, *389*, 506–516.

[7] Bi, Q.Y.; Lin, J.D.; Liu, Y.M.; He, H.Y.; Huang, F.Q.; Cao, Y. Dehydrogenation of formic acid at room temperature: Boosting palladium nanoparticle efficiency by coupling with pyridinic-nitrogen-doped carbon. *Angew. Chem. Int. Ed.* 2016, *55*, 11849–11853.

[8] Li, Z.; Yang, X.; Tsumori, N.; Liu, Z.; Himeda, Y.; Autrey, T.; Xu, Q. Tandem nitrogen functionalization of porous carbon: Toward immobilizing highly active palladium nanoclusters for dehydrogenation of formic acid. *ACS Catal.* 2017, *7*, 2720–2724.

[9] Kim, Y.; Kim, D.H. Hydrogen production from formic acid dehydrogenation over a Pd supported on N-doped mesoporous carbon catalyst: A role of nitrogen dopant. *Appl. Catal. A Gen.* 2020, *608*, 117887.

[10] Wang, J.-Y.; Kang, Y.-Y.; Yang, H.; Cai, W.-B. Boron-doped palladium nanoparticles on carbon black as a superior catalyst for formic acid electro-oxidation. *J. Phys. Chem. C* 2009, *113*, 8366–8372.

[11] Jiang, K.; Xu, K.; Zou, S.; Cai, W.-B. B-doped Pd catalyst: Boosting room-temperature hydrogen production from formic acid–formate solutions. *J. Am. Chem. Soc.* 2014, *136*, 4861–4864.

[12] Li, H.; Qin, X.; Zhang, X.-G.; Jiang, K.; Cai, W.-B. Boron-doped platinum-group metals in electrocatalysis: A perspective. *ACS Catal.* 2022, *12*, 12750–12764.

[13] Koh, K.; Jeon, M.; Yoon, C.W.; Asefa, T. Formic acid dehydrogenation over Pd nanoparticles supported on amine-functionalized SBA-15 catalysts: Structure–activity relationships. *J. Mater. Chem. A* 2017, *5*, 16150–16161.

[14] Navlani-García, M.; Mori, K.; Kuwahara, Y.; Yamashita, H. New approaches toward the hydrogen production from formic acid dehydrogenation over Pd-based heterogeneous catalysts. *Front. Mater.* 2019, *6*, 44.

[15] Miao, X.; Meng, Y.; Li, X.; Deng, X.; Li, Y.; Xiao, J. Highly efficient hierarchical porous carbon supported Pd-based catalyst for formic acid dehydrogenation. *Catalysts* 2022, *12*, 240.

[16] Cao, T.; Cheng, J.; Ma, J.; Yang, C.; Yao, M.; Liu, F.; Deng, M.; Wang, X.; Ren, Y. Facile synthesis of microporous carbons from biomass waste as high-performance supports for dehydrogenation of formic acid. *Nanomaterials* 2021, *11*, 3028.

[17] Duan, Z.; Zhang, Y.; Liu, Y.; Wang, G.; Li, Q. Highly efficient hydrogen evolution from formic acid using B,N co-doped carbon supported palladium catalysts. *Appl. Surf. Sci.* 2023, *614*, 156205.

[18] Chen, Z.; Li, X.; Liu, J.; Wang, Y.; Zhang, H.; Ma, D. Designing a robust palladium catalyst for formic acid dehydrogenation. *ACS Catal.* 2023, *13*, 10299–10310.

[19] Díaz-Herrezuelo, I.; García-Suárez, E.J.; Bedia, J.; Rodriguez, J.J.; Gómez-Sainero, L.M. Three-dimensional palladium/activated-carbon-based catalysts for continuous hydrogen production from formic acid. *J. Mater. Chem. A* 2023, *11*, 25278–25290.

[20] Liu, H.; Huang, M.; Tao, W.; Han, L.; Zhang, J.; Zhao, Q. A palladium catalyst supported on boron-doped porous carbon for efficient dehydrogenation of formic acid. *Nanomaterials* 2024, *14*, 549.

[21] Qi, X.; Liu, Y.; Zhang, J.; Zhao, Z.; Wang, C. Potential–rate correlations of supported palladium-based catalysts for aqueous-phase formic acid dehydrogenation. *ACS Catal.* 2024, *14*, 4745–4758.

[22] Abdel-Fattah, T.M.; Biehler, E.; Smeaton, M.; Gennett, T.; Leick, N. Photo-induced hydrogen production from formic acid using a palladium catalyst. *Catalysts* 2025, *15*, 213.